We are IntechOpen, the world's leading publisher of Open Access books Built by scientists, for scientists

6,900
Open access books available

186,000
International authors and editors

200M
Downloads

Our authors are among the

154
Countries delivered to

TOP 1%
most cited scientists

12.2%
Contributors from top 500 universities

CLARIVATE ANALYTICS
BOOK CITATION INDEX
INDEXED

WEB OF SCIENCE™

Selection of our books indexed in the Book Citation Index
in Web of Science™ Core Collection (BKCI)

Interested in publishing with us?
Contact book.department@intechopen.com

Numbers displayed above are based on latest data collected.
For more information visit www.intechopen.com

Chapter

Femtosecond Electron Diffraction Using Relativistic Electron Pulses

Jinfeng Yang

Abstract

Observation of atomic-scale structural motion in matter with femtosecond temporal resolution is of considerable interest to scientists and paves the way for new science and applications. For this purpose, ultrafast electron diffraction (UED) imaging using femtosecond electron pulses is a very promising technique, as electrons have a larger elastic scattering cross section as compared to photons or X-rays and can be easily focused in observation with high spatial resolution. In this chapter, we first give an overview of the historical development of current nonrelativistic UEDs and discuss the potentials of UEDs with relativistic electron pulses. Second, we describe the concept and development of relativistic UED with femtosecond electron pulses generated by a radio-frequency acceleration-based photoemission gun. Some demonstrations of diffraction imaging of crystalline materials using 3-MeV electron pulses with durations of ∼100 fs are presented. Finally, we report a methodology of single-shot time-resolved diffraction imaging for the study of ultrafast dynamics of photo-induced irreversible phase transitions.

Keywords: ultrafast electron diffraction, femtosecond electron pulse, relativistic electron beam, structural dynamics, radio-frequency electron gun

1. Introduction

Femtosecond imaging is a long-awaited technique for materials scientists to observe atomic and molecular motions directly and in real time. For this type of ultrafast imaging, time-resolved diffraction with short-pulsed X-rays has been developed and is widely used globally. Recently, ultrafast electron diffraction (UED) using femtosecond electron pulses [1–3] has facilitated the study of the structural dynamics of reversible and irreversible processes, including ultrafast phase transformations, femtosecond chemical/biochemical reactions, and radiation damages. It is well-known that electrons have many advantages over X-rays. Electrons have a larger elastic scattering cross section and can be easily focused to develop a measurement with high spatial resolution. A small sample can be used in the UED measurement. The instruments used with UEDs are also very compact.

The earliest time-resolved electron diffraction experiments with pulsed electrons on the milli- to microsecond time scale were developed using a deflection technique in the 1980s [4]. Later, a photoemission pulsed electron source was used in an electron diffraction measurement by Ewbank et al. [5, 6]. The temporal resolution was improved to sub-nanoseconds. In 1982, Mourou and Williamson [7] pioneered the use of 100-ps electron pulses to construct a picosecond electron

diffraction experiment. Later, they used a streak-camera tube to generate 25-keV picosecond electron pulses ($\sim$20 ps) in a UED experiment and succeeded at detecting laser-induced ultrafast phase transformation in aluminum [8]. The number of electrons per pulse used in the diffraction measurement was maintained at $\sim 10^4$. Since 2000, the research groups of Zewail [1, 9, 10], Miller [2], and Cao [11] have focused their efforts on generating ultrashort electron pulses. A mode-locked femtosecond laser was used to generate ultrashort electron pulses and to excite the samples. A temporal resolution of sub-picoseconds and femtoseconds was achieved in UEDs, which provided real-time diffraction imaging and enabled the recording of atomic or molecular motion in chemical and biochemical reactions. **Figure 1** shows a schematic of a typical femtosecond electron-diffraction apparatus constructed with a laser-driven electron source, magnetic lens, sample-positioning system, and electron diffraction detector. In most UEDs, a conventional Ti:sapphire femtosecond pulsed laser is used to generate ultrashort electron pulses with a photocathode and to pump the sample to induce structural changes in materials. The key elements of this apparatus are the electron source and detection system.

The temporal resolution is mainly defined by the electron pulse duration. In all of the aforementioned UEDs, a DC acceleration-based photoemission electron gun was used to generate ultrashort electron pulses with a short-pulsed laser. The use of a higher accelerating electric field (extraction field, E_{ext}) between the photocathode and anode (grid) is crucial to reducing Coulomb repulsion of electrons (space-charge effects). The transit-time broadening τ_{KE} can be reduced by increasing E_{ext}, because $\tau_{KE} \propto \sqrt{\Delta E_{kin}}/E_{ext}$ [12], where ΔE_{kin} is the kinetic energy spread of photo-electrons. For an Au or Ag photocathode driven by a 266-nm ultraviolet (UV) laser, $\Delta E_{kin} \sim 0.6$ eV, the dispersive broadening near the photocathode can be maintained below 300 fs at E_{ext} = 10 MV/m or more [3]. However, the maximum static extraction field in the dc gun is determined by the vacuum breakdown limit of $\sim$10 MV/m.

The space-charge effects occur not only in the electron gun but also during the propagation of the electron pulse from the gun to the sample. The broadening of both the pulse duration and energy spread of electrons due to the space-charge effects in the propagation of nonrelativistic femtosecond electron pulses has been investigated theoretically by Siwick et al. [13]. Their results indicated that when
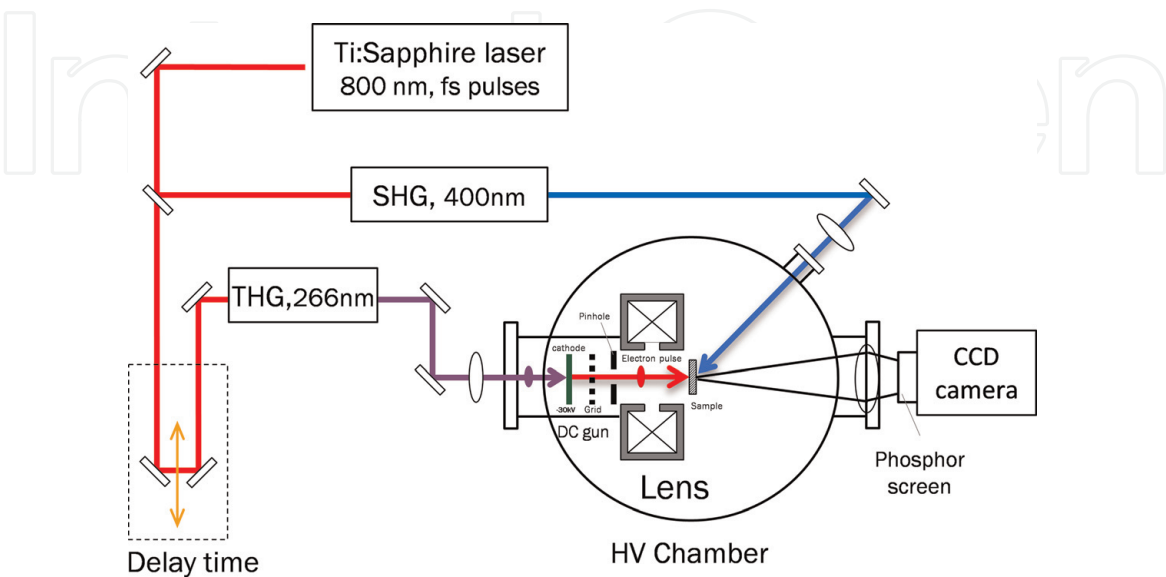

Figure 1.
Schematic of a typical femtosecond electron-diffraction apparatus. A DC-acceleration-based photoemission electron gun is used to produce ultrashort electron pulses with third harmonics of a Ti:sapphire femtosecond laser. The electron pulse passes through the specimen and produces a diffraction pattern of the structure.

a 30-keV and 300-fs electron pulse containing $\sim 10^4$ electrons is transported to the sample with a 40-cm-long drift space, the pulse duration is increased to 4 ps, and the relative energy spread is increased to 3×10^{-3}. In this case, both the temporal and spatial resolutions are reduced by the space-charge effects. To reduce the space-charge effects, two solutions are used in UED. One involves a decrease in the number of electrons in the pulse. This results in a low brightness electron beam at the sample and presents tremendous difficulties for single-shot imaging in the study of the dynamics of irreversible processes. Another involves reducing the photocathode-to-sample distance. Miller et al. at the University of Toronto developed a 30-keV electron gun with a photocathode-to-sample distance of 4.5 cm. This source produced a 600-fs short electron pulse containing 6000 electrons per pulse. The beam fluence at the sample $\varphi = N/A$, where N is the total number of electrons per pulse and A is the beam area at the sample, is $\varphi \sim 1 \times 10^{11} \text{ m}^{-2}$ [14]. Nevertheless, a minimum of $\sim 10^4$–10^5 electrons per pulse are needed to resolve the diffraction peak and/or obtain a clear image in UED [15].

To generate high-brightness electron beams with pulse durations on the order of 100 fs, an advanced accelerator technology for radio-frequency (RF) acceleration-based photoemission electron guns (photocathode RF guns) has been proposed to generate multi-MeV femtosecond electron pulses for UED [16–27]. The RF gun is usually operated with a high RF electric field equal to or >100 MV/m. Therefore, the electrons emitted from the photocathode can be quickly accelerated into the relativistic energy region to minimize the space-charge effects in the pulse, yielding a femtosecond or picosecond pulse with numerous electrons. Recently, Yang et al. [28–30] developed the first prototype for relativistic ultrafast electron microscopy using the RF gun. They succeeded in generating high-brightness electron pulses with a pulse duration of 100 fs containing 10^7 electrons at an energy of 3 MeV. They also demonstrated the single-shot imaging using these femtosecond electron pulses [31, 32]. Relativistic UED is very promising for the study of ultrafast dynamics in solid-state materials and chemical/biological complex systems. It exhibits many crucial advantages over nonrelativistic UED systems:

- High-current electron pulses enable single-shot imaging so that both reversible and irreversible processes in materials can be observed.

- Higher energies considerably enhance the extinction distance for elastic scattering and provide structural information that is essentially free from multiple scattering and inelastic effects. This enables us to easily understand and explain structural dynamics.

- Ultrashort pulses of <100 fs are possible. The utilization of the relativistic electron pulse overcomes the loss of temporal resolution because of the velocity mismatch in samples. High temporal resolution of 100 fs or less can be achieved in relativistic UED.

- A thick sample can be used for measurement, thus obviating the requirement to prepare suitable thin samples.

- Radiation effects derived from ionization damage processes decrease at higher energies in samples. In fact, at MeV energies, the dominant damage process for electron beams is not ionization but rather the much slower ballistic "knock-on" process.

- Relativistic UED is suitable for in situ observations, as large areas exist in the sample room for installing various specimens. Relativistic UED can be used to study gas-, liquid-, and solid-phase samples.

In this chapter, we introduce UED with relativistic femtosecond electron pulses. The chapter also describes the generation of femtosecond electron pulses using an RF photoemission gun, the concept and design of relativistic UED, and demonstration experiments with relativistic femtosecond electron pulses.

2. Relativistic UED with femtosecond electron pulses

Relativistic UED consists of a 1.6-cell S-band (2.856 GHz) photocathode RF gun, an imaging system with magnetic lenses, a femtosecond laser, and a detector. **Figure 2** shows a schematic and photograph of relativistic UED at Osaka University. All components were installed on a vibration-controlled board with a size of 3×3 m^2.
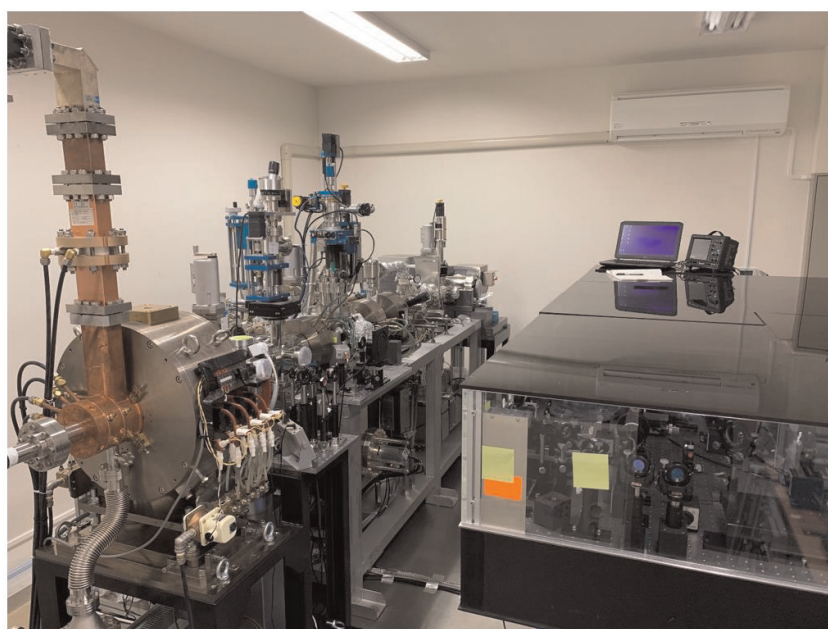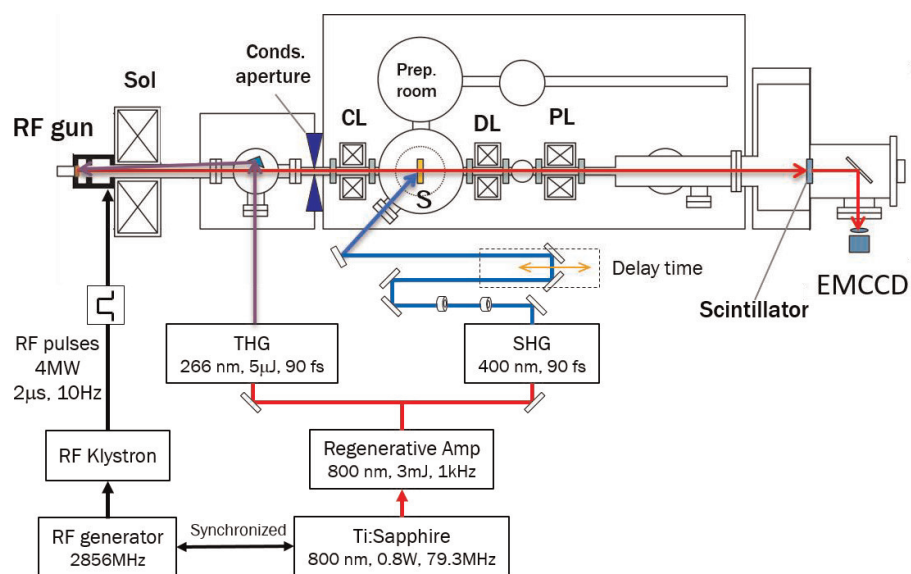

Figure 2.
Schematic (top) and photograph (bottom) of UED apparatus with relativistic femtosecond electron pulses at Osaka University. All components are installed on a vibration-controlled board with a size of 3×3 m^2.

2.1 Photocathode RF gun

The photocathode RF gun is a high-brightness electron source and has been widely applied in the field of advanced particle accelerators (e.g., free-electron lasers and linear colliders). The RF gun used in relativistic UED consists of two RF cavities: a half cell and a full cell (1.6-cell), as shown in **Figure 3**. The length of the full-cell cavity is equal to half the 2.856 GHz RF wavelength, $\lambda/2$ = 52.48 mm, whereas the length of the half cell is 0.6 times $\lambda/2$; numerical studies have shown that an optimal performance is obtained if the half-cell cavity is 0.6 times the full cell length rather than 0.5×. The design and details of the cavities were described in [32, 33]. The cavities are driven by a MW-power 2.856 GHz accelerating RF to produce a stronger accelerating RF field on the photocathode. The RF gun is operated in the TM_{010} transverse magnetic mode [34, 35]. The phase shift between the half and full cells is equal to π, resulting in the acceleration of electrons in both cavities. The linear components of the electric fields at r = 0 (the center axis of the RF cavities) [32] can be assumed to be:

$$E_z = E_0 \cos kz \sin (\omega t + \varphi_0), \qquad (1)$$

where E_0 is the peak accelerating field, $k = 2\pi/\lambda$, $\omega = ck$, c is the velocity of light, and ϕ_0 is the initial RF phase when the electron leaves the cathode surface (z = 0) at t = 0. In relativistic UED, the peak RF power filled to the RF cavities is 4 MW, resulting in E_0 = 75 MV/m. This field thus accelerates electrons emitted from the photocathode quickly up to 3 MeV to minimize the space-charge effects in the pulses. Therefore, the RF gun can easily produce femtosecond electron pulses by the illumination of the femtosecond laser on the photocathode.

The visualization of atomic-scale structural motion by UED requires electron pulses of the shortest duration and lowest emittance to achieve high temporal and spatial coherence. The temporal resolution of UED is determined based on the duration of the electron pulses. The beam emittance directly determines the quality of the diffraction image (e.g., the sharpness of the diffraction patterns (DPs) and the diffraction contrast in the acquired images (i.e., spatial resolution)). The pulse duration and emittance of the electron beam are two crucial parameters in UED.

2.1.1 The temporal duration of the electron pulses

The temporal duration of the electron pulses generated from the RF gun, in the absence of time delay due to the response time of the photocathode materials, is
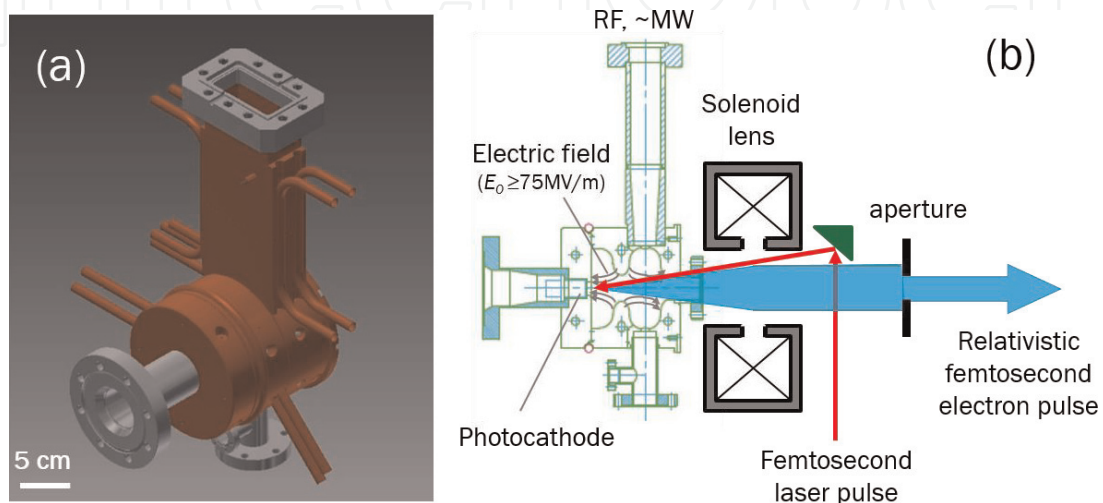

Figure 3.
(a) Photocathode RF gun and (b) schematic for the generation of femtosecond electron pulses in the RF gun.

given by the driving laser pulse duration and temporal electron broadening. The temporal electron broadening can be defined with two components: one derives from the initial energy bandwidth (initial kinetic energy spread, ΔE_{kin}) of electrons emitted from the photocathode, as described in Section 1. Another derives from the space-charge-induced broadening during the propagation from the cathode to the sample. Therefore, the electron pulse duration can be given as

$$\sigma_b = \sqrt{\sigma_{opt}^2 + \tau_{KE}^2 + \tau_{SC}^2}, \tag{2}$$

where σ_b is the pulse duration of electrons, σ_{opt} is the laser pulse duration, and τ_{KE} and τ_{SC} are the temporal broadenings due to the initial kinetic energy spread and space-charge effect, respectively. The first temporal broadening is proportional to $\tau_{KE} \propto \sqrt{\Delta E_{kin}}/E_{acc}$ [12], where E_{acc} is the accelerating electric field (E_{ext} in the dc gun and E_0 for the RF gun). The second temporal broadening is proportional to Q/E^2, where Q and E are the electron charge and total energy of the electron beam, respectively. For the 3-MeV electron pulses at $Q < 1$ pC, τ_{KE} and τ_{sc} in the RF gun are negligible. Therefore, the duration of low-charge electron pulses generated from the RF gun is approximately equal to the driving laser pulse duration, $\sigma_b \approx \sigma_{opt}$.

2.1.2 The total emittance of the electron beam

The total emittance of the electron beam generated from the RF gun [32] is given as:

$$\varepsilon = \sqrt{\varepsilon_{rf}^2 + \varepsilon_{sc}^2 + \varepsilon_{th}^2}, \tag{3}$$

$$\varepsilon_{rf} = 2.73 \times 10^{-11} E_0 f^2 \sigma_x^2 \sigma_b^2, \tag{4}$$

$$\varepsilon_{sc} = 3.76 \times 10^3 \frac{Q}{E_0(2\sigma_x + \sigma_b)}, \tag{5}$$

where ε_{rf} is the normalized RF-induced emittance in root mean square (RMS) in mm-mrad, ε_{sc} is the normalized RMS space-charge-induced emittance in mm-mrad, ε_{th} is the thermal emittance (initial emittance) at the cathode, E_0 is the peak accelerating field in MV/m, f is the RF in MHz, Q is the electron charge of the pulse in nC, and σ_b and σ_x are the RMS pulse duration in ps and RMS transverse beam size in mm, respectively. For example, under the conditions of $E_0 = 75$ MV/m, $\sigma_b = 100$ fs, $\sigma_x = 0.3$ mm, and $Q = 0.1$ pC (10^6 electrons per pulse), we estimate that $\varepsilon_{rf} = 1.5 \times 10^{-5}$ mm-mrad and $\varepsilon_{sc} = 7 \times 10^{-3}$ mm-mrad. This indicates that the RF-induced emittance is negligible and the magnitude of the space-charge-induced emittance at $Q \leq 0.1$ pC is close to the order of nm-rad. Therefore, in this case, the thermal emittance (initial emittance) at the cathode is dominant.

Assuming an isotropic emission into a half sphere in front of the cathode surface, the thermal emittance can be expressed in terms of the RMS incident laser spot size on the cathode σ_r and the initial kinetic energy spread ΔE_{kin} of the photoelectrons:

$$\varepsilon_{th} = \sigma_r \sqrt{\frac{2\Delta E_{kin}}{3m_0 c^2}}, \tag{6}$$

where m_0 is the electron mass and σ_r is the laser spot size at the photocathode. For a very fine copper photocathode driven by a 266-nm laser under the conditions of $E_0 = 75$ MV/m and $\phi_0 = 30°$, $\Delta E_{kin} = 0.42$ eV [36]. Therefore, the thermal

emittance is estimated as a function of the RMS laser spot size: $\varepsilon_{th} = 0.74 \times \sigma_r$. This indicates that we can reduce the emittance to $\varepsilon_{th} \sim 10$ nm-rad in the RF gun if we can focus the laser spot as $\sigma_r = 10$ μm at the photocathode. In this case, the peak brightness of electron pulses B_p can be calculated by

$$B_p = (\beta\gamma)^2 \frac{Q}{\varepsilon^2 \sigma_b}, \tag{7}$$

where $\beta = v/c$, v is the electron velocity, and γ is the normalized relativistic energy. From a 3-MeV electron pulse with a pulse duration of 100 fs, we can calculate the peak brightness to $B_p = 5 \times 10^{17}$ A/m^2 sr and the beam fluence to $\varphi \sim 2 \times 10^{11}$ m^{-2}. The spatial coherence length can be calculated by [37]:

$$L_c = \frac{h}{m_0 c} \frac{\sigma_x}{\varepsilon}, \tag{8}$$

where h is Planck's constant. If $\sigma_x = 0.3$ mm at the sample, the spatial coherence length is $L_c \sim 10$ nm, which is an ideal value for electron diffraction imaging. It is twice as large or greater than that of current nonrelativistic UED systems [12, 37, 38]. This allows us to detect sharp DPs and acquire good contrast diffraction images in the measurements.

In the presented relativistic UED apparatus, a very fine copper photocathode was used and illuminated by the third-harmonic of a Ti:sapphire laser (266 nm, pulse duration: 90 fs). The pulse energy of the UV light was 5 μJ at maximum. The diameter of the laser spot at the photocathode was 0.1 mm in RMS focused by an optical lens. The injection phase (gun phase) was 30°, which is an optimal condition to minimize the transverse emittance. The electron beam energy was 3 MeV under the 4-MW RF input. The repetition rate of the electron pulses was 10 Hz, which was determined by the repetition rate of the RF pulses.

2.2 UED imaging system

2.2.1 Electron illumination system

The electron illumination system consists of a solenoid magnetic lens, condenser lens, and condenser aperture to control and transfer the electron pulses from the RF gun on the specimen, as shown in **Figure 3**. The solenoid lens with a large beam aperture is used to create a parallel electron beam. The condenser aperture made of a 1-mm-thick molybdenum metal with four pinholes with diameters of 0.3, 0.5, 1, and 2 mm stops the large-divergence electrons to further reduce the emittance, yielding a small illumination convergence angle at the specimen. After the aperture, we use the condenser lens to create a parallel beam or convergent beam on the specimen. The parallel beam is used for selected area diffraction, whereas the convergent beam is used mainly for convergent beam electron diffraction.

The emittance of the electron beam that passed through the aperture with 0.5, 1 and 2 mm diameter pinholes was measured as 0.1, 0.3, and 0.7 mm-mrad [30], respectively. Reducing the emittance increased the RMS brightness in the pulse. The RMS brightness of the transmitted electrons was 2.2, 1.4 and 0.5×10^{22} electrons/ m^2 sr, and the number of electrons per pulse was ~ 0.6, 2.5, and 4.4×10^7 at the sample with 0.5-, 1-, and 2-mm diameter pinholes, respectively. For the use of the 0.3-mm-diameter pinhole, the number of electrons in the pulse was $\sim 1 \times 10^6$, and the brightness was estimated to be $\geq 5 \times 10^{22}$ electrons/m^2 sr. The illumination convergence angle of the electron beam at the sample was $\alpha = 26$ μrad in the

parallel-beam operation mode with the 0.3-mm-diameter condenser aperture, which is discussed in a later section.

The specimen room is located downstream of the condenser lens. The distance from the photocathode to the specimen is 1.2 m. The sample is manipulated by six-axis motorized stages. In a time-resolved experiment, the sample can be pumped by a femtosecond laser pulse, as shown in **Figure 2**. A pump laser with wavelengths of 266, 400, and 800 nm can be selected to meet the requirements of the measured materials. The pulse duration of the pump laser pulses is 90 fs in full width at half maximum (FWHM). The vacuum pressure in the specimen room reaches $\sim 10^{-10}$ Torr. When inserting or changing a new sample, the sample is first installed into a separated vacuum chamber (preparation room) for the sample cleaning.

2.2.2 Imaging system

The diffraction imaging system consists of a diffraction lens (DL) and a projection lens (PL). The diffraction lens focuses the electrons at a back focal plane (BFP), yielding the DPs on the BFP. The projection lens then projects the DPs in the desired magnification onto a viewing screen (scintillator) through a charge-coupled device (CCD) camera, as shown in **Figure 4**. An aperture with a pinhole diameter of 0.5 mm is inserted at the DL center to block scattered electrons and scattered pump laser light. The UED patterns can be observed in two modes: a wide-momentum mode, in which the PL is weak or turned off, and a high-resolution mode, in which the PL magnifies the DPs or images onto the scintillator.

To achieve a high sensitivity to MeV electron detection with a high damage threshold, a Tl-doped CsI columnar crystal scintillator equipped with a fiber optic plate (Hamamatsu Photonics) is used to convert the relativistic-energy DPs or images into optical images. Finally, the optical images are propagated by a thin reflective mirror (at 45°) and detected with an electron-multiplying CCD (EMCCD) with 1024×1024 pixels. The effective detection area of the scintillator is 50×50 mm^2, whereas the distance from the specimen to the scintillator is 1.6 m. The sensitivity of the whole detection system is 3×10^{-3} counts/electron. The intensity and position of Bragg peaks in the DPs can be monitored and recorded simultaneously using analysis software for studying the structural dynamics.
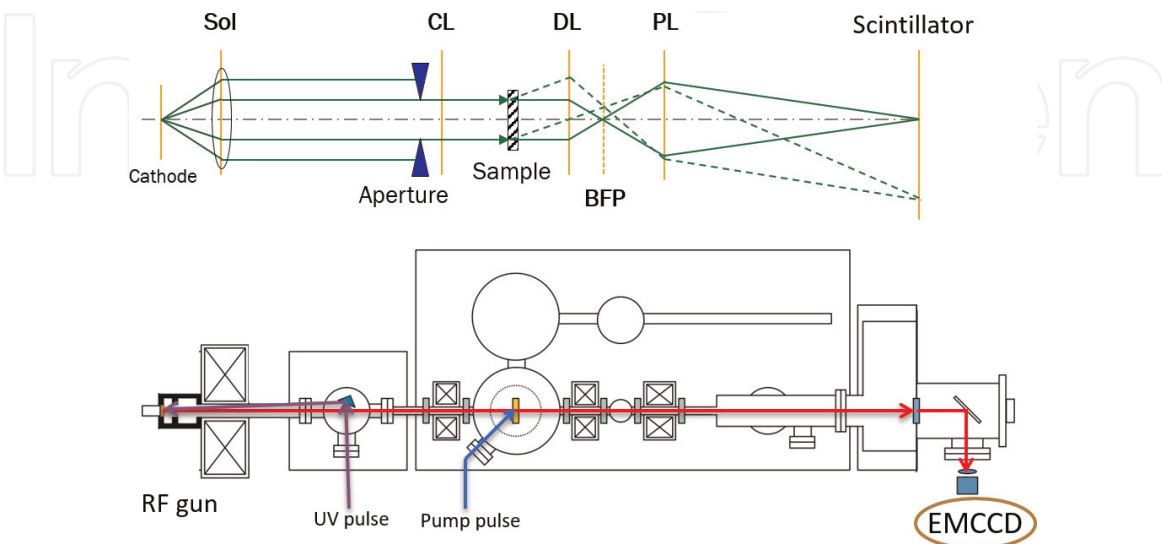

Figure 4.
Schematic of UED imaging with a parallel beam (parallel beam configuration). DL focuses the electrons at a BFP, yielding DPs on BFP. PL then projects the DPs in the desired magnification onto the scintillator. The DPs can be observed in two modes: a wide-momentum mode, in which the PL is weak or turned off, and a high-resolution mode, in which the PL magnifies the DPs or images onto the scintillator.

2.3 Femtosecond laser system

A conventional mode-locked Ti:sapphire femtosecond laser (Spectra-Physics) is used to illuminate the photocathode and to excite the sample. The laser consists of a 80-fs Ti:sapphire laser oscillator (Tsunami, central wavelength: 800 nm) and a regenerative amplifier (Spitfire Ace) that includes a pulse stretcher and compressor. The femtosecond laser oscillator is synchronized to an external 79.3-MHz RF signal with a time-to-lock piezoelectric device, as shown in **Figure 2**. The 79.3-MHz RF signal is generated by dividing the accelerating 2856-MHz RF by 1/36. The time jitter between the laser pulse and RF phase is <100 fs. The laser oscillator output is fed to the regenerative amplifier for pulse stretching, amplification, and compression. The regenerative amplifier is driven by a green laser with a repetition rate of 1 kHz (Empower, wavelength: 532 nm, output: 20 W). The pulse energy of the amplifier output is 3 mJ. The pulse duration is 90 fs in FWHM after the pulse compression.

The amplified femtosecond laser beam is divided into two beams. One is converted to the third-harmonics by a wavelength converter (Tripler) composed of two nonlinear crystals (SHG and THG) and a time plate for pulse delay adjustment. The third-harmonic pulses (UV wavelength, 266 nm; pulse duration, ~90 fs) with a maximum energy of 5 μJ per pulse are focused by an optical lens and then illuminated onto the copper photocathode to generate femtosecond electron pulses. The residual fundamental femtosecond laser (wavelength: 800 nm) is used directly to excite the sample or is converted to second-harmonics (wavelength: 400 nm) or third-harmonics (wavelength: 266 nm) to excite the sample, based on the sample's requirements. The time delay between the pump laser pulse and the probe electron pulse is changed with an optical delay located on the pump laser beam line for time-resolved experiments, as shown in **Figure 2**. The repetition rate of the pump laser pulses is reduced to 10 Hz with two optical choppers, similar to the repetition rate of the electron pulses.

3. UED experiments with relativistic femtosecond electron pulses

3.1 Observations of DPs from crystalline metals, semiconductors, and chemical compounds

In relativistic UED, we measured the DPs of various crystalline materials (e.g., metals, semiconductors, and chemical compounds). The electron pulses generated from the RF gun were collimated by the condenser aperture with the different pinhole diameters of 1, 0.5, and 0.3 mm before the sample was illuminated. The energy and pulse durations of the electron pulses were 3 MeV and ~100 fs, respectively. The following four samples were used:

1. 35-nm-thick single-crystalline silicon (Si) films produced from a 60-μm-thick Si (001) wafer by photolithography and plasma etching

2. 30-nm-thick polycrystalline aluminum foils (Cat. No. S108, EM-Japan)

3. Polycrystals of a thallous chloride chemical compound dispersed on a carbon film pasted on a copper mesh (Cat. No. S110, EM-Japan)

4. Multilayer single-crystalline mica films

All DPs of the four samples were observed under the wide-momentum mode.

Figure 5 shows the DPs of a (001)-orientated single-crystalline Si sample observed both through single-pulse (single-shot) and 10-pulse integrations. A condenser aperture with a 0.3-mm-diameter pinhole was used to collimate the electron beam. The number of electrons in the pulse was $\sim 1 \times 10^6$. In **Figure 5a**, both the lowest Bragg and higher-order peaks clearly appear in the single shot. The excellent quality of the diffraction image is much higher than the pioneering data in the nonrelativistic UED measurement [22]. In **Figure 5b**, entire DPs are clearly visible with 10 pulses integrated. The maximum scattering vector is more than 2 Å^{-1}.

The intensity profile of Bragg peaks along (440) and (−4–40) spots of the single-shot image is shown in **Figure 5c**. The RMS width of the zeroth-order spot (000) was 0.015 Å^{-1}, indicating an excellent spatial resolution for the MeV diffracted beam. Based on the width of the (000) spot and the measured distance of the diffraction spots from the (000) position, we estimated the RMS illumination convergence angle of the electron beam at the specimen to be α = 26 μrad. By using the 0.3-mm-diameter condenser aperture, we improved both the width and convergence angle from the previous development [20]. The RMS width of both the (220) and (−2–20) diffraction spots, which included the effects of the probe beam energy spread, was identical to that of the (000) spot, indicating a small energy spread in the electron pulse generated by the RF gun.
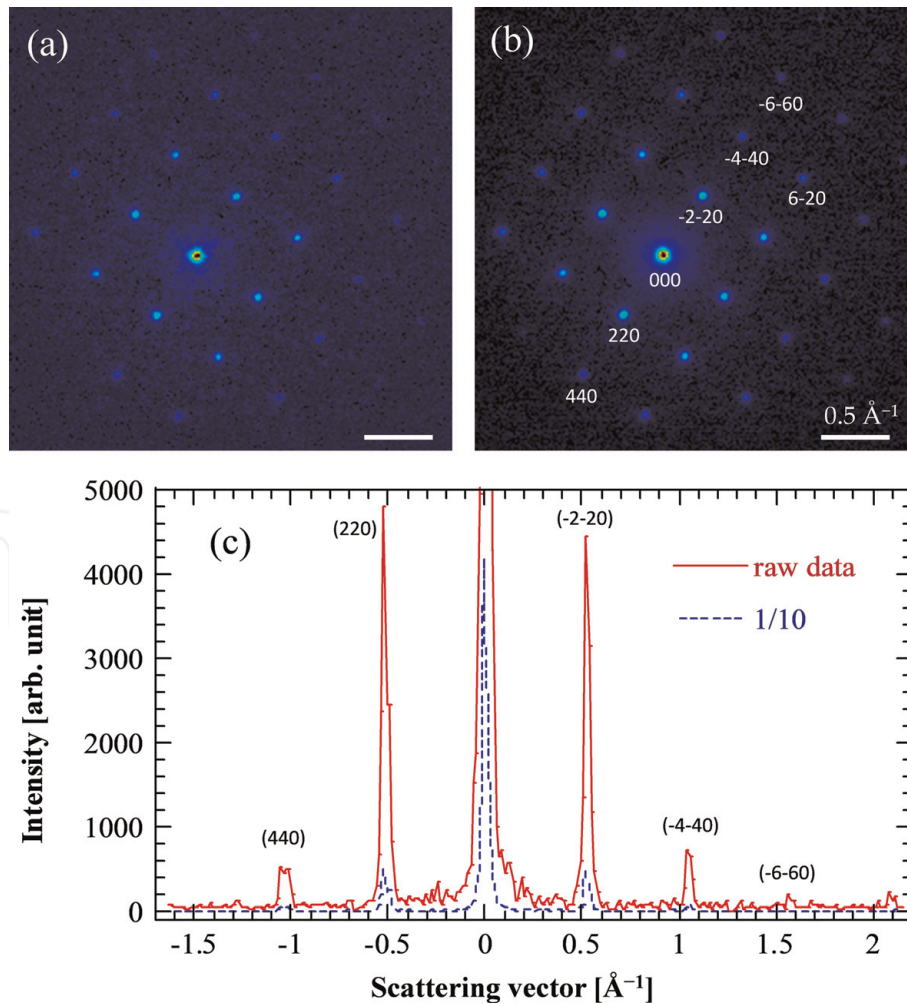

Figure 5.
DPs of a (001)-oriented single-crystalline Si measured with (a) single-shot and (b) 10-pulse integrations. (c) The intensity profile along (440) and (−4–40) spots of the single-shot image. The solid line represents the raw data, and the broken line is given with 1/10 intensities. The energy of the electron pulses is 3 MeV, containing approximately 1×10^6 electrons per pulse.

Figure 6 shows transmission electron microscopy (TEM) images and UED patterns of a 30-nm-thick polycrystalline aluminum foil (top images) and polycrystalline thallous chloride (bottom images). The DPs were measured with single-shot and 100-pulse integrations. The energy of the electron pulses was 3 MeV. The condenser aperture with a 1-mm diameter pinhole was used to collimate the electrons. The number of electrons in each pulse was 2.5×10^7. The demonstrations indicate that relativistic UED also enabled the electron diffraction imaging of polycrystalline materials and chemical compounds, and the entire DPs were clearly visible with 100 pulses. These suggest that UED with relativistic femtosecond electron pulses enables the study of ultrafast chemical reactions in chemistry and biology. Moreover, single-shot imaging is also possible for polycrystalline materials. This means that the irreversible processes and reactions in polycrystalline materials and chemical compounds can be observed using relativistic UED.

Figures 7 shows the DPs of a (100)-oriented multilayer single-crystalline mica measured with single-shot, 10-, and 100-pulse integrations [29]. The energy of the electron pulses was 3 MeV. The condenser aperture with a 0.5-mm-diameter pinhole was used to collimate the electrons. The number of electrons in the pulse was 6×10^6. The mica sample was composed of a chemical compound of $KAl_2(AlSi_3)O_{10}(OH)_2$ with a multilayer structure. The thickness of the monolayer was ~10 Å. This is used widely to check the performance of electron diffraction observation in TEM. In general, diffraction imaging of mica is difficult comparing with that of metallic single crystals because of the close diffraction spots. In the relativistic UED measurement as shown in Figure 7, both the lowest Bragg and higher-order peaks clearly appear in the observation with 10-pulse integration, and the entire DPs are readily obtained with 100 pulses. Moreover, the possibility of single-shot observation is shown in the measurement.
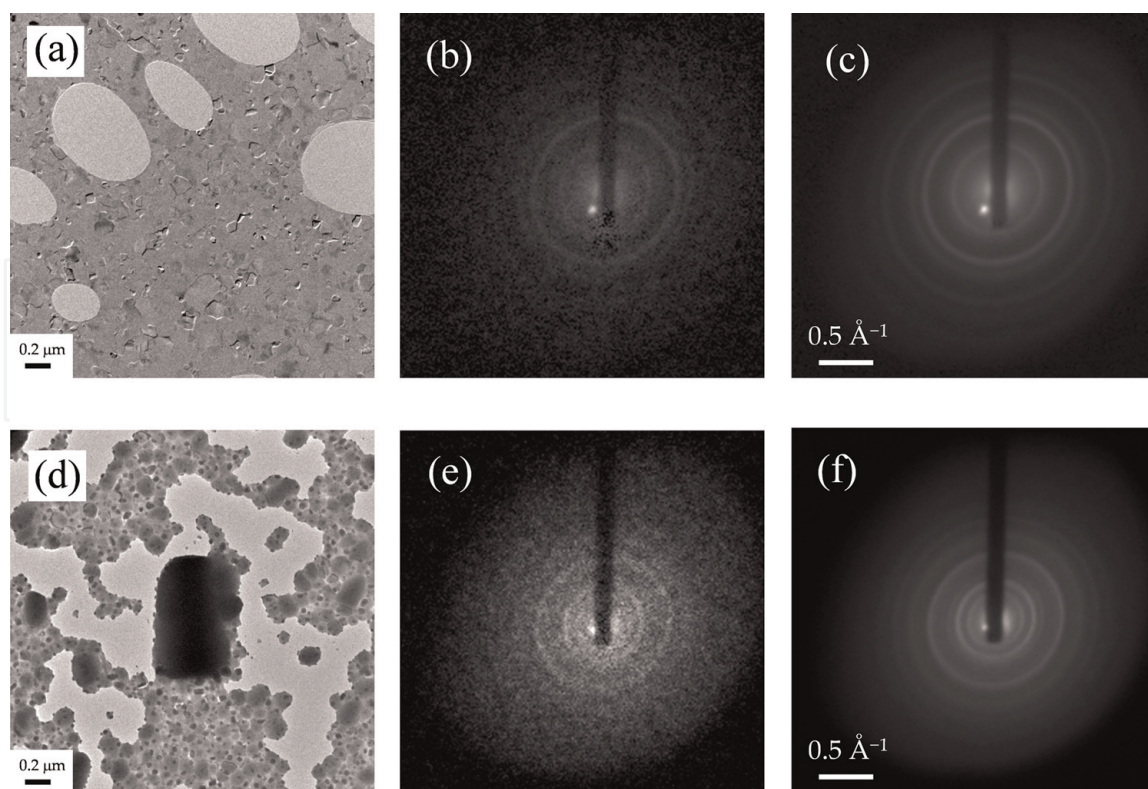

Figure 6.
TEM and UED images. Top: a 30-nm thick polycrystalline Al foil. Bottom: polycrystalline thallous chloride. The images of (a) and (b) are measured by a 200-KV TEM. The DPs of (b) and (e) are measured with single-shot, whereas (c) and (f) are measured with 100-pulse integration. The energy of the electron pulses is 3 MeV, containing 2.5×10^7 electrons per pulse.
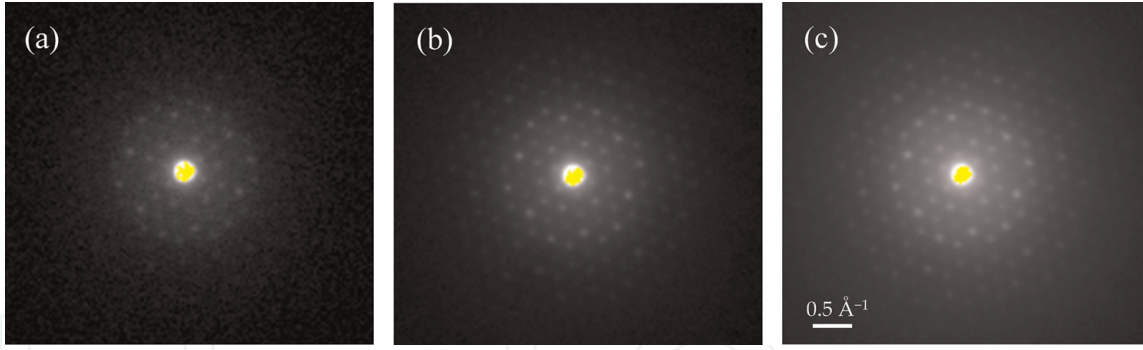
Figure 7.
DPs of a (100)-oriented multilayer single-crystalline mica measured with (a) single-shot, (b) 10-, and (c) 100-pulse integrations [29]. The energy of the electron pulses is 3 MeV, containing 6×10^6 electrons per pulse.

In summary, the experiments indicated that (1) the relativistic UED with femtosecond electron pulses can be applied to electron diffraction imaging of a wide range of materials and (2) relativistic UED enables single-shot observation with femtosecond electron pulses. This means that the ultrafast dynamics of irreversible processes in materials can be measured using relativistic UED.

3.2 Time-resolved measurement for study of ultrafast structural dynamics

A time-resolved measurement technique is used in UED to observe the structural dynamics in a sample. In this case, a femtosecond laser pulse with the desired wavelength based on the sample's requirement is used to excite the sample, whereas the electron pulses are used as a probe to monitor the DPs as a function of the time delay between the pump laser pulse and electron pulse. The time delay in the measurement is adjusted by an optical delay placed on the pump laser beam line, as shown in **Figure 2**. The pulse energy and polarization of the pump laser can be changed to meet the requirements. In the absence of a velocity mismatch between the pump and the probe beams within the sample, the final temporal resolution of UED is expressed as:

$$\Delta t = \sqrt{\sigma_b^2 + \sigma_l^2 + \Delta t_j^2}, \tag{9}$$

where σ_b is the probe electron pulse duration, σ_l is the pump laser pulse duration, and Δt_j represents the time jitter between two pulses. The time jitter in the relativistic UED is determined by the synchronization of the laser pulse to the accelerating RF phase. Therefore, we can define $\Delta t_j < 100$ fs, as discussed in Section 2.3. In the presented time-resolved experiment, both the durations of the pump and probe pulses are ~100 fs in RMS, yielding a total temporal resolution of ~180 fs in RMS.

The intensities of Bragg peaks measured in the UED experiments reflect both the lattice temperature effect (in terms of the Debye-Waller factor) and details of the structural changes. For example, by monitoring the intensities of Bragg peaks as a function of the time delay between the two pulses, we can investigate the phase transformation in materials (e.g., melting of metal excited by laser light). **Figure 8** presents an example of a time-resolved UED experiment to observe laser-induced melting dynamics in a 10-nm-thick (001)-oriented single-crystal gold film [25, 26]. The sample was excited by a 385-nm femtosecond laser (second-harmonic of a turned 770-nm Ti:sapphire laser). The UED patterns were observed by 3-MeV electron pulses. The electron pulses were collimated to a 200-µm diameter by an aperture in the front of the sample. The diameter of the pump laser at the sample was 800 µm, which was much larger than that of the probe electron beam. The
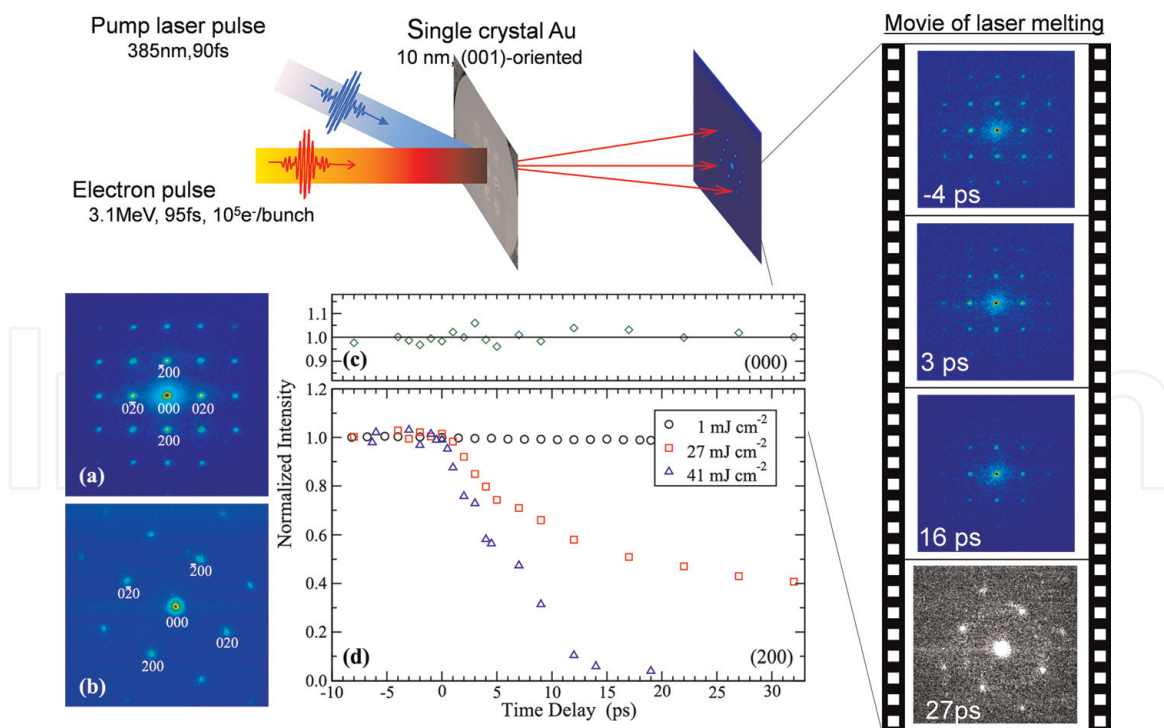
Figure 8.
Schematic and results of a time-resolved UED experiment. The UED patterns (a) and (b) are obtained by wide-momentum and high-resolution modes, respectively. (c) The (000)-order peak intensity was obtained by single-shot at F = 27 mJ/cm². (d) The (200) Bragg peak intensities at F = 1, 27 and 41 mJ/cm² were obtained by averaging over four equivalent (200) Bragg-peak spots [25]. Copyright 2013, with permission from the American Institute of Physics.

temporal resolution of the pump-probe measurement was ~180 fs. **Figure 8d** gives the plot of the (200) Bragg peak intensity as functions of the pump laser fluence (F) and the time delay between the probe and pump pulses. The intensity was normalized with respect to the value measured for each sample prior to laser excitation. At $F = 27$ mJ/cm², 40% of the intensity was still detectable after 30 ps, whereas the intensity was nearly reduced to zero within ~15 ps at $F = 45$ mJ/cm², indicating a strong dependence on the excitation fluence.

To determine the structural changes in the film reflected in the measured dynamics of Bragg peaks, we applied a hybrid method that combines the two-temperature model with classical molecular dynamics (2 T-MD) [26]. This method has already been used to model the laser-induced melting of nanofilms and nanorods. By comparing the theoretical predictions from 2 T-MD with the UED measurements, we succeeded in revealing the mechanism of the laser-induced melting. **Figure 9** shows a comparison of experimental and theoretical signals at the pump laser fluences of 27 and 41 mJ/cm² and the cross sections of the atomistic simulation of melting in the single-crystal gold film at the absorbed fluences (F_{abs}) of 3.0 and 4.5 mJ/cm². The model reproduced both the fast decay of Bragg intensity at <5 ps and the slower longer-term behavior. At low fluence, $F = 27$ mJ/cm² or $F_{abs} = 3.0$ mJ/cm² (**Figure 9a** and **c**), the dynamics exhibited premelting of free surfaces and heterogeneous melting by melt front propagation. The melt fronts slowly propagated toward the center, but the film did not melt entirely, and small regions of crystalline gold remained at 1.2 ns. At high fluence, $F = 41$ mJ/cm² or $F_{abs} = 4.5$ mJ/cm² (**Figure 8b** and **d**), the sample expanded more rapidly, and the premelting was more pronounced. The average temperature reached the melting temperature at 6 ps, and homogenously distributed seeds of low-density molten phase were subsequently created at 6–12 ps. When the sample reached the limit of crystal stability (after 12 ps), these molten seeds grew and coalesced until the sample melted entirely ~20 ps.
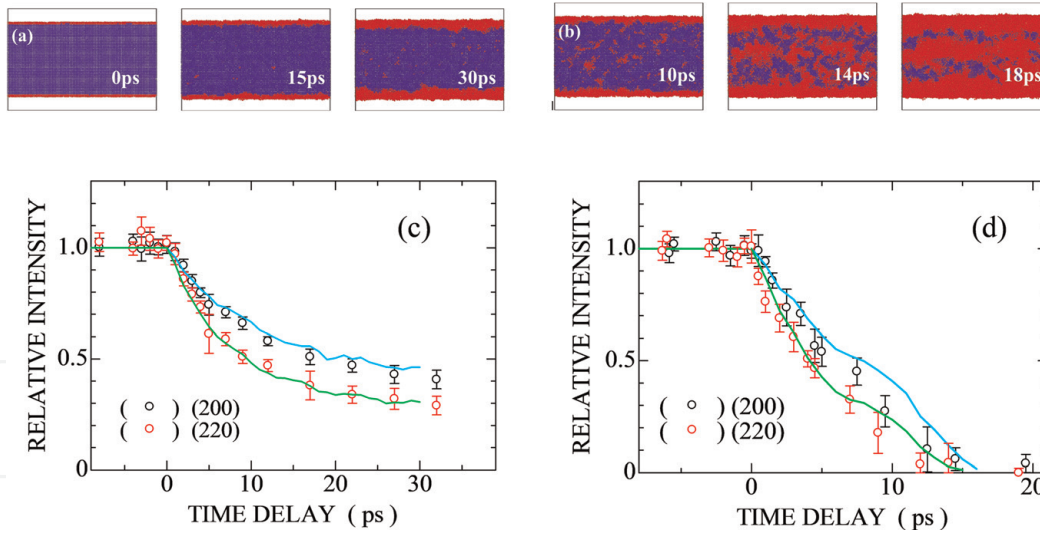
Figure 9.
Cross-sections (top) of the atomistic simulation of meltings in single crystal gold films at (a) F_{abs} = 3.0 and (b) 4.5 mJ/cm^2, and a comparison (bottom) of experimental and theoretical signals as a function of time delay at (c) F = 27 and (d) 41 mJ/cm^2. The dots denote the experimental data, whereas the lines represent the theoretical results. In (a) and (b), all atoms are color-coded according to the measure of a degree of crystallinity given by the (nearest-neighbor averaged) centro-symmetry parameter Φ. Blue atoms ($\Phi < 0.45$) have a local crystalline structure, and red atoms ($\Phi \geq 0.45$) have highly disordered surroundings [25]. Copyright 2013, with permission from the American Institute of Physics.

Recently, other time-resolved observations of ultrafast structural dynamics in semiconductors, organic crystals, and two-dimensional materials have been proposed in relativistic UED. The results showed that relativistic UED has great potential and excellent performance for the study of ultrafast photo-induced phase transitions.

4. Conclusion

In this chapter, we introduced femtosecond diffraction imaging with relativistic electron pulses. We also discussed relativistic femtosecond electron pulse generation using an RF-acceleration-based photoemission gun, a relativistic UED apparatus, and demonstrations of UED measurements with the relativistic femtosecond electron pulses. The electron pulses generated by the RF gun exhibited excellent characteristics, including a low emittance of ≤0.1 mm-mrad, a short pulse duration of 100 fs, and a high number of electrons of ≥10^6 in the pulse at an energy of 3 MeV. The peak brightness was reached at 10^{22} electrons/m^2 sr. These pulses facilitated (1) the acquisition of high-quality DPs with a spatial resolution of 0.015 Å^{-1} and (2) a time-resolved experiment (pump-probe measurement) with an excellent temporal resolution of 180 fs. The most important result was the single-shot observation with relativistic femtosecond electron pulses in a wide range of materials. The findings suggest that relativistic UED is very promising for the study of ultrafast dynamics of irreversible processes and chemical reactions (not discussed in this chapter) in the femtosecond time region.

In addition, the UED system is also very stable because it combines the current state-of-the-art femtosecond mode-locked laser and RF-acceleration and time-synchronization technologies. In our study, the fluctuation of the Bragg peak intensity was <5% in the long term (i.e., 24 hours or more). The relativistic UED apparatus is also very compact.

In the future, an ultralow emittance of ∼10 nm-mrad can be expected by focusing the μm-diameter laser spots on the photocathode and collimating the

electron beam with a small condenser aperture of 0.1 mm or less. In this case, the spatial coherence length can be improved to $L_c > 10$ nm, which is an ideal value for electron diffraction imaging with the highest spatial resolution. In addition, as discussed in Section 3.2, the atomic-level analytical method of 2 T-MD is very useful to explain the atomic dynamics and underlying mechanisms. Through combination with the 2 T-MD method, relativistic UED can be a powerful tool for femtosecond imaging in materials science, chemistry, and biology.

Acknowledgements

Author details

Jinfeng Yang
The Institute of Scientific and Industrial Research, Osaka University, Osaka, Japan

*Address all correspondence to: yang@sanken.osaka-u.ac.jp

IntechOpen

References

[1] Zewail AH. 4D ultrafast electron diffraction, crystallography, and microscopy. Annual Review of Physical Chemistry. 2006;**57**:65-103. Available from: https://www.annualreviews.org/doi/10.1146/annurev.physchem.57.032905.104748

[2] Siwick BJ, Dwyer JR, Jordan RE, Dwayne Miller RJ. An atomic-level view of melting using femtosecond electron diffraction. Science. 2003;**302**: 1382-1385. DOI: 10.1126/science.1090052

[3] King WE et al. Ultrafast electron microscopy in materials science, biology, and chemistry. Journal of Applied Physics. 2005;**97**:111101. DOI: 10.1063/1.1927699

[4] Rood AP, Milledge J. Combined flash-photolysis and gas-phase electron-diffraction studies of small molecules. Journal of the Chemical Society, Faraday Transactions II. 1984;**80**: 1145-1153. Available from: https://pubs.rsc.org/en/content/articlepdf/1984/f2/f29848001145

[5] Ewbank JD et al. Instrumentation for gas electron diffraction employing a pulsed electron beam synchronous with photoexcitation. The Review of Scientific Instruments. 1992;**63**: 3352-3358. DOI: 10.1063/1.1142552

[6] Lobastov VA et al. Instrumentation for time-resolved electron diffraction spanning the time domain from microseconds to picoseconds. The Review of Scientific Instruments. 1998; **69**:2633-2643. DOI: 10.1063/1.1148991

[7] Mourou GA, Williamson S. Picosecond electron diffraction. Applied Physics Letters. 1982;**41**:44-45. DOI: 10.1063/1.93316

[8] Williamson S, Mourou G, Li JCM. Time-resolved, laser-induced phase transformation in aluminium. Physical Review Letters. 1984;**52**:2364-2367. DOI: 10.1103/PhysRevLett.52.2364

[9] Ihee H et al. Direct imaging of transient molecular structures with ultrafast diffraction. Science. 2001;**291**: 458-462. DOI: 10.1126/science.291.5503.458

[10] Williamson JC et al. Clocking transient chemical changes by ultrafast electron diffraction. Nature. 1997;**386**: 159-162. DOI: 10.1038/386159a0

[11] Cao J et al. Femtosecond electron diffraction for direct measurement of ultrafast atomic motions. Applied Physics Letters. 2003;**83**:1044-1046. DOI: 10.1063/1.1593831

[12] Aidelsburger M, Kirchner FO, Krausz F, Baum P. Single-electron pulses for ultrafast diffraction. PNAS. 2010;**107**:19714-19719. DOI: 10.1073/pnas.1010165107

[13] Siwick BJ, Dwyer JR, Jordan RE, Dwayne Miller RJ. Ultrafast electron optics: Propagation dynamics of femtosecond electron packets. Journal of Applied Physics. 2002;**92**:1643-1648. DOI: 10.1063/1.1487437

[14] Siwick BJ, Dwyer JR, Jordan RE, Dwayne Miller RJ. Ultrafast electron optics: Propagation dynamics of femtosecond electron packets. Chemical Physics. 2004;**299**:285-305. DOI: 10.1016/j.chemphys.2003.11.040

[15] Sciaini G, Dwayne Miller RJ. Femtosecond electron diffraction: Heralding the era of atomically resolved dynamics. Reports on Progress in Physics. 2011;**74**:096101. DOI: 10.1088/0034-4885/74/9/096101

[16] Hassan MT. Attomicroscopy: From femtosecond to attosecond electron microscopy. Journal of Physics B:

Atomic, Molecular and Optical Physics. 2018;**51**:032005. DOI: 10.1088/1361-6455/aaa183

[17] Hastings JB, Rudakov FM, Dowell DH, Schmerge JF, Cardoza JD, Castro JM, et al. Ultrafast time-resolved electron diffraction with megavolt electron beam. Applied Physics Letters. 2006;**89**:184109. DOI: 10.1063/1.2372697

[18] Li RK, Tang CX, Du YC, Huang WH, Du Q, Shi JR, et al. Experimental demonstration of high quality MeV ultrafast electron diffraction. The Review of Scientific Instruments. 2009;**80**:083303. DOI: 10.1063/1.3194047

[19] Musumeci P, Moody JT, Scoby CM. Relativistic electron diffraction at the UCLA Pegasus photoinjector laboratory. Ultramicroscopy. 2008;**108**:1450-1453. DOI: 10.1016/j.ultramic.2008.03.011

[20] Murooka Y, Naruse N, Sakakihara S, Ishimaru M, Yang J, Tanimura K. Transmission-electron diffraction by MeV electron pulses. Applied Physics Letters. 2011;**98**:251903. DOI: 10.1063/1.3602314

[21] Zhu P, Zhu Y, Hidaka Y, Wu L, Cao J, Berger H, et al. Femtosecond time-resolved MeV electron diffraction. New Journal of Physics. 2015;**17**:063004. DOI: 10.1088/1367-2630/17/6/063004

[22] Harb M, Peng W, Sciaini G, Hebeisen CT, Ernstorfer R, Eriksson MA, et al. Excitation of longitudinal and transverse coherent acoustic phonons in nanometer free-standing films of (001) Si. Physical Review B. 2009;**79**:094301. DOI: 10.1103/PhysRevB.79.094301

[23] Shen X, Li RK, Lundstrom U, Lane TJ, Reid AH, Weathersby SP, et al. Femtosecond mega-electron-volt electron microdiffraction.

Ultramicroscopy. 2018;**184**:172-176. DOI: 10.1016/j.ultramic.2017.08.019

[24] Fu F, Liu S, Zhu P, Xiang D, Zhang J, Cao J. High quality single shot ultrafast MeV electron diffraction from a photocathode radio-frequency gun. The Review of Scientific Instruments. 2014;**85**:083701. DOI: 10.1063/1.4892135

[25] Giret Y, Naruse N, Daraszewicz SL, Murooka Y, Yang J, Duffy DM, et al. Determination of transient atomic structure of laser-excited materials from time-resolved diffraction data. Applied Physics Letters. 2013;**103**:253107. DOI: 10.1063/1.4847695

[26] Daraszewicz SL, Giret Y, Naruse N, Murooka Y, Yang J, Duffy DM, et al. Structural dynamics of laser-irradiated gold nanofilms. Physical Review B. 2013;**88**:184101. DOI: 10.1103/PhysRevB.88.184101

[27] Yang J, Kan K, Naruse N, Yoshida Y, Tanimura K, Urakawa J. 100-femtosecond MeV electron source for ultrafast electron diffraction. Radiation Physics and Chemistry. 2009;**78**:1106-1111. DOI: 10.1016/j.radphyschem.2009.05.009

[28] Yang J, Yoshida Y, Shibata H. Femtosecond time-resolved electron microscopy. Electronics and Communications in Japan. 2015;**98**:50-57. DOI: 10.1002/ecj.11763

[29] Yang J. Ultrafast electron microscopy using relativistic-energy femtosecond electron pulses. Microscopy. 2015;**50**:156-159. Available from: http://microscopy.or.jp/jsm/wp-content/uploads/publication/kenbikyo/50_3/50_3e04jy.html

[30] Yang J, Yoshida Y, Yasuda H. Ultrafast electron microscopy with relativistic femtosecond electron pulses. Microscopy. 2018;**67**:291-295. DOI: 10.1093/jmicro/dfy032

[31] Yang J, Yoshida Y. Relativistic ultrafast electron microscopy: Single-shot diffraction imaging with femtosecond electron pulses. Advances in Condensed Matter Physics. 2019; **2019**:9739241. DOI: 10.1155/2019/9739241

[32] Arita M, Sakaguchi N. Electron microscopy: Novel microscopy trends. In: Yang J, editor. Ultrafast Electron Microscopy with Relativistic Femtosecond Electron Pulses. InTechOpen; 2019. DOI: 10.1093/jmicro/dfy032

[33] Kan K, Yang J, Kondoh T, Yoshida Y. Development of femtosecond photocathode RF gun. Nuclear Instruments and Methods in Physics Research Section A. 2011;**659**: 44-48. DOI: 10.1016/j.nima.2011.08.016

[34] Terunuma N, Murata A, Fukuda M, Hirano K, Kamiya Y, Kii T, et al. Improvement of an S-band RF gun with a Cs_2Te photocathode for the KEK-ATF. Nuclear Instruments and Methods in Physics Research Section A. 2010;**613**: 1-8. DOI: 10.1016/j.nima.2009.10.151

[35] Yang J, Sakai F, Yanagida T, Yorozu M, Okada Y, Takasago K, et al. Low-emittance electron-beam generation with laser pulse shaping in photocathode radio-frequency gun. Journal of Applied Physics. 2002;**92**: 1608-1612. DOI: 10.1063/1.1487457

[36] Yang J, Kan K, Kondoh T, Murooka Y, Naruse N, Yoshida Y, et al. An ultrashort-bunch electron RF gun. Journal of the Vacuum Society of Japan. 2012;**55**:42-49. DOI: 10.3131/jvsj2.55.42

[37] Van Oudheusden T, de Jong EF, van der Geer SB. Op't root WPEM, Luiten OJ. Electron source concept for single-shot sub-100 fs electron diffraction in the 100 keV range. Journal of Applied Physics. 2007;**102**:093501. DOI: 10.1063/1.2801027

[38] Gahlmann A, Park AT, Zewail AH. Ultrashort electron pulses for diffraction, crystallography and microscopy: Theoretical and experimental resolutions. Physical Chemistry Chemical Physics. 2008;**10**: 2894-2909. DOI: 10.1039/b802136h